

QUALITY ASSESSMENT OF UAV PHOTOGRAMMETRIC ARCHAEOLOGICAL SURVEY

S. Barba^a, M. Barbarella^b, A. Di Benedetto^c, M. Fiani^a, M. Limongiello^a

^aDepartment of Civil Engineering, University of Salerno, Fisciano (SA), Italy
(sbarba; m.fiani; mlimongiello)@unisa.it;

^bDepartment of Civil, Chemical, Environmental and Materials Engineering - ARCES, University of Bologna, Bologna, Italy
maurizio.barbarella@unibo.it

^cDepartment of Civil Engineering, Roma Tre University, Roma, Italy
alessandro.dibenedetto@uniroma3.it

Commission II

KEY WORDS: Reprojection errors, Amphitheatre of Avella, 3D model, GNSS measurement.

ABSTRACT:

The paper reports the results of a photogrammetric survey made using an Unmanned Aerial Vehicle (UAV) in the archaeological site of the Roman Amphitheatre in Avella (Avellino, Italy). The aim of the study is to verify which modality of image acquisition (if only nadiral images or nadiral plus Oblique images), together with the method of Global Positioning Satellite System (GNSS) survey of the Ground Control Points (GCP) is able to produce the better 3D model, in terms of accuracy, in order to extract traditional graphic drawings (plan, elevation and section), suited to the required representation scales (1:100 and 1:50). The accuracy in georeferencing was evaluated analysing the residues on the GCPs; subsequently, a more detailed analysis of the accuracy of the final 3D model was performed analysing the residuals on the image coordinates, also called re-projection error. The method developed is based on the statistical analysis of the different models, built changing the GCPs survey method and the photogrammetric shots acquired. The results of our analysis show that the photogrammetric survey is more 'stable' using only nadiral images and that the nRTK technique allows results comparable to those obtained with static measurements, both in precision and in reliability. Moreover, if the GCPs are measured in nRTK mode, taking into consideration the graphical error, the maximum representation scale is 1:100, whereas the use of static technique makes it possible to describe major details, at a scale of 1:50.

1. INTRODUCTION

For the last decade, the use of photogrammetry for digital 3D recording has undergone a considerable increase of the applications. In fact, thanks to the evolution of algorithms coming from Computer Vision and new calculation techniques, the photogrammetry sped up and automated the processing time, which used to be a well-known weak point.

With the passing of time, the overall situation gradually transitioned from the common use of scientific applications for 3D surveying with dense clouds realized with the laser scanner technology, to an increasing use of photogrammetry, thanks to the introduction of the automatic Structure of Motion technology.

Nowadays, the photogrammetric technique gained even more 'vitality', probably overcoming in a number of applications the range-based sensors. More recently, the technological development of UAVs (Unmanned Aerial Vehicles), are day-by-day getting easier to drive and more reliable, indirectly favoured the increase in photogrammetric applications, especially in applications on medium and large scale.

It can be said that, since 2000, drones have become more suitable for aerial photography, and the first studies on the quality of the results were released concurrently (Eisenbeiß, 2009).

In the literature, UAV systems for photogrammetric purposes were often used in the archaeological field for the three-dimensional survey of complex structures such as the Roman Amphitheatres.

The factors that favoured the acquisitions with UAVs, compared to the more classical ones (TLS - Terrestrial Laser Scanner, for example), are mainly: a lower instrument cost, a greater speed of data collection in the field and above all a better colorimetric result of the 3D model, necessary for a

correct analysis and archaeological characterization (Remondino et al., 2011; Rinaudo et al., 2012).

In the literature there are many applications of aerophotogrammetric surveys from UAVs, for Theatres and Amphitheatres from the Roman era, such as the Theatre of Ventimiglia (Nocerino et al., 2013), the Amphitheatre and the Theatre of the Augusta Bagiennorum area (Chiabrando et al., 2011, Bendea et al., 2007), the Theatre and the Amphitheatre of the Pompeii archaeological park (Saleri et al., 2013, Fiorillo et al., 2016), or outside the Italian context, the Ancient Nikopolis Theatre (Bilis et al., 2017) in Greece or the Amphitheatre of Carnuntum in Austria (Verhoeven et al., 2013).

Often, the scale of representation of graphic products, obtained from a photogrammetric process, does not take into account the residues on the Ground Control Points (GCP) and/or Check Point (CP).

In fact, knowing the definition of the graphic error, the maximum scale of representation is inversely proportional to the metric errors computed on the model (Cardone, 2015).

A well-known problem in a photogrammetric project is indeed the georeferencing phase, specifically the choice of the instrumentation and its way to use to obtain the maximum precision on the model. A low precision of the model can nullify a high resolution of the data, and consequently, the graphic scale of the products (i.e. plans, sections, elevations). The aim of the study on the Amphitheatre is to verify which type of acquisition of photogrammetric shots (only nadiral images or nadiral plus Oblique images), together with the type of GCP measurement (based on GNSS techniques), produces the 3D model with less metric residues, in order to extract traditional graphic drawings (plan, elevation and section), suited to the required representation scales.

2. AVELLA'S PROJECT

The activity of survey, study and analysis on the archaeological site was carried out as part of the project "The Amphitheatre of the Avella, from its origins to the digital: architecture, landscape, virtual representation, innovations for knowledge and fruition" (Limongiello et al., 2016). The layout of the complex, made of two external semi-circular structures joined by orthogonal walls and of an internal oval-shaped arena, covers an area of 63.6 x 34.3 m.

The dimensions document a site smaller than the better-known amphitheatre of Pompeii, although these values could lead to a default estimate of the real extensions since the northern and eastern sectors show a poor state of conservation in their outer regions. The *cavea* develops on three orders: the *ima cavea*, the *media cavea*, the *summa cavea* (Fig. 1). The few remains of the latter one is located on the south and east sides, while the *media cavea*, divided into three parts (*moeniana*, *praecintiones* and *baltei*) is still in a good state of confinement. The Amphitheatre, similar in composition to the complex located in Pompeii, is one of the oldest in Campania. Unlike the more recent sites, like the Colosseum in Rome or the Flavio Amphitheatre in Pozzuoli, there are no underground passages but only two monumental entrances, consisting of vaulted hallways in *opus caementicium* placed on opposite sides of the main axis: *Porta Triumphalis*, (north) and *Porta Libitinensis* (south), both paved with stone slabs.

The project purpose is a first digitization of the Amphitheatre, producing 3D models suitable for a cartographic restitution (consisting of plans and sections) in 1:100 and 1:50 scale. Due to the high metric quality of the required documents, it has been necessary to pay attention to the metric error of the photogrammetric model with respect to accurate topographic measurements made during the campaign phase.

3. DATA ACQUISITION

3.1 Photogrammetric shots by UAV

The UAV system used for this application is a hexacopter assembled (Fig. 2) with a net weight of the sensor of about 2.3 kg and maximum payload of 1 kg. The installed camera is a mirrorless Sony Nex 7 with 24-megapixel APS-C sensor (6000 x 4000 pixels, 23.5 x 15.6 mm and a Pixel Size of 3.96 μm) and a fixed Sony E-Mount lens (16 mm focal length, Field of View - FOV 83°).

For the acquisition of the photogrammetric shots, a double capture mode was chosen: a first one using an automatic flight plan for the acquisition of nadiral photogrammetric shots, and a second one in manual mode with the camera's optical axis inclined of about 45°, to film the vertical walls and any shadow cones present between the *cavea*. The image acquisition was planned bearing in mind the project requirements - a GSD of about 1cm - and, at the same time, with the aim of guaranteeing a high level of automation in the next step of data elaboration.

The images were acquired in time-lapse mode (interval of 2 seconds), for a total 626 images, 435 of which by automatic flight plan and camera in Nadir, while the other 191 with a manual flight and optical camera axis inclined at 45°. The Nadir flight was developed from north-west to southeast, with an average height of flight of 32 m above the arena plan, which provides a ground coverage of about 47.0 x 31.2 m.

The manual flight with a tilted camera and an average height of flight of 21, which provides a not constant ground coverage, varies between 16.0 x 11.0 m and 23.5 x 15.6 m, respectively. The acquired images were processed in two different projects: a first one containing only the Nadir images (435), and a second one containing, in addition to the nadiral images, also the Oblique ones (435 plus 191).



Figure 1: The Amphitheatre of Avella (Italy).



Figure 2: The employed UAV for the photogrammetric aerial survey.

In Figures 3 and 4 the details of the "camera positions" are shown.

3.2 GNSS survey

Photogrammetric acquisition was supported and combined with GNSS positioning techniques. The spatial distribution of GCPs in the different acquisition modes is shown in Figure 5. In this test, we proceeded to measure natural (well defined) and artificial targets in two different modalities:

- A. fast - static network consisting of 8 natural points well distributed and altimetrically staggered (A1-A8, in black);
- B. nRTK network consisting of 17 natural targets (A1-A17, in yellow);
- C. nRTK network consisting of 22 artificial targets placed on the ground (P1-P22, in black).

The first two modalities (A and B), have 8 points in common (A1 to A8); the targets size is 42 x 29.7 cm (A3 format), with a coded target (Schneider, 1991). The GNSS survey refers to the Italian geodetic and cartographic System UTM/ETRF00 (Barbarella, 2014) through a connection to two permanent stations (AVEL and ROBS) included in the national Geodetic Network located within a radius of 10km from the test area. A new point (master) has been materialized near the Amphitheatre and connected to the

permanent stations with static baselines. Some GCPs were measured by the Master station (about 50 m apart) with GNSS bases. These same points and all other GCPs were measured with nRTK technique. The instrumentation used to measure each target consists of an antenna with a built-in receiver of the Geomax (a Geomax Zenith 25); instead, a Zenith antenna with a separate Trimble receiver was used to measure the master station. The processing of GNSS measurements in static mode was carried out using the "Geomax Geo Office" software, produced by Geomax. In Fig. 6 was been reported a GNSS measurement phase, while Table 1 were showed the RMS GNSS measurement.

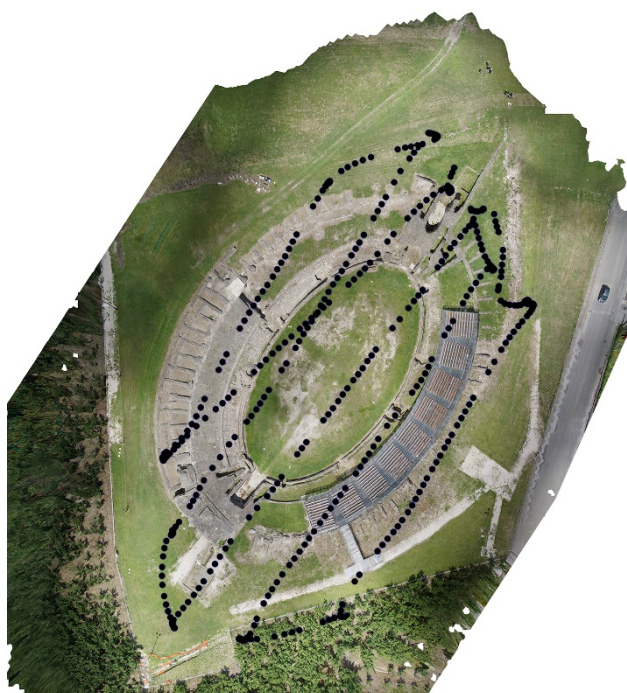


Figure 3: Ortophoto Nadir and camera positions Hexacopter (only Nadir images).



Figure 4: Ortophoto Nadir and camera positions Hexacopter (only Oblique images).

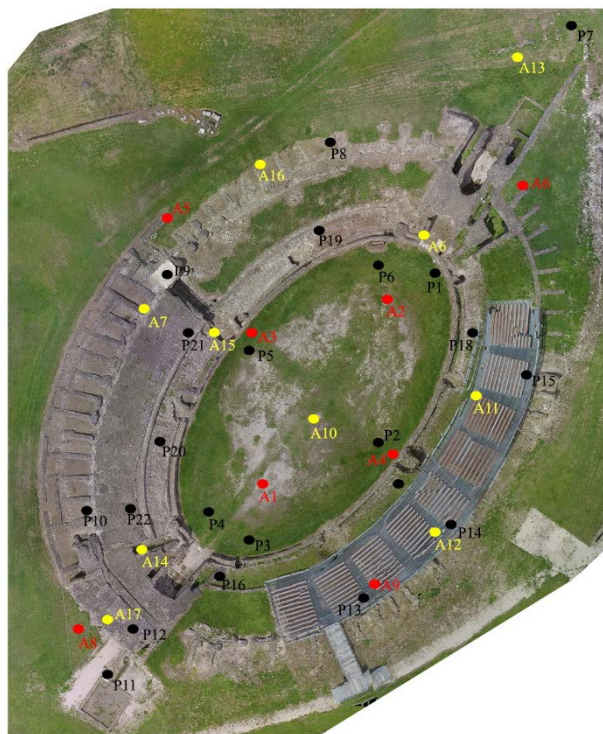


Figure 5: GCP in two different modalities: black (nRTK measurement on target), red (fast-static measurement on natural points), and yellow (nRTK measurement on natural points).



Figure 6: GCP measurement phase: right panel on photogrammetric targets, left panel on natural points.

Tab. 1: RMSE

	$RMSE_{E,N}$ [mm]	RMS_h [mm]
Static	4÷5	12
nRTK	8	15

4. METHODS

4.1 Analysis of accuracy

The required accuracy is a function of the scale of representation, proportional to the graphic error. The verification of the graphic

error is necessary to define the maximum representation scale of the surveyed object.

The choice of the best solution in terms of accuracy was made analysing two main configurations for photogrammetric data:

- Processing using only nadiral images;
- Processing using the same nadiral images combined with Oblique images.

For both photogrammetric configurations, the GCPs were measured with the GNSS system in fast - static and nRTK modalities, both on photogrammetric targets and on clearly visible natural points.

In the framework of this test, Agisoft PhotoScan software (version 1.3.2 build 4164, Agisoft, 2016) was employed, which is one of the most popular tools used for 3D reconstruction purposes in the international community.

The method developed is based on the statistical analysis of the different models, changing the GCP measurement typology and the photogrammetric shots acquired.

The accuracy in georeferencing was evaluated analysing the residues on the GCPs; subsequently, a more detailed analysis of the accuracy of the final 3D model was performed analysing the residuals on the image coordinates, also called reprojection error computed values within the adjustment process, therefore, this is the accuracy of the Tie-Points after the optimization by the bundle adjustment with the GCPs coordinates. The Tie-Points extraction was performed using a modified SIFT (scale-invariant feature transform, (Lowe, 2004) approach. Eventually the external orientation (bundle block adjustment) was performed using the most common algorithm of the computer vision community, namely the Gauss - Markov approach (Rothermel et al., 2012).

For the analysis of the geo-referencing residuals on the GCPs, the RMSE estimates on the coordinates and their combination were considered:

$$RMSE_E = \sqrt{\frac{1}{n} \cdot \sum_{i=1}^n (\bar{E}_{C_i} - E_{R_i})^2}$$

$$RMSE_N = \sqrt{\frac{1}{n} \cdot \sum_{i=1}^n (\bar{N}_{C_i} - N_{R_i})^2}$$

$$RMSE_h = \sqrt{\frac{1}{n} \cdot \sum_{i=1}^n (\bar{h}_{C_i} - h_{R_i})^2}$$

$$RMSE = \sqrt{RMSE_E^2 + RMSE_N^2 + RMSE_h^2}$$

where the subscript *C* indicates the coordinates estimated from the bundle adjustment whereas *R* indicates the reference values. A reprojection error is the distance between a Tie-Point measured on a calibrated image, and a corresponding object point projected onto the same image. In general, if the overall mean reprojection error is too high, the images with the highest error must be excluded and the instrument recalibrated; reprojection error is also referred to as RMS (Root Mean Square) image residual (James et al., 2017a). In Agisoft manual, reprojection error is defined as the distance between the point on the image where a reconstructed 3D point can be projected, and the original projection of that 3D point detected on the photo. Theoretically, reprojection error is obtained as follows:

$$w \begin{pmatrix} u \\ v \\ 1 \end{pmatrix} = \begin{pmatrix} f_u & 0 & u_c \\ 0 & f_v & v_c \\ 0 & 0 & 1 \end{pmatrix} \left(R_c^T - R_c^T t_c \right) \begin{pmatrix} P \\ 1 \end{pmatrix} = KP_c \begin{pmatrix} P \\ 1 \end{pmatrix}$$

where: f_u and f_v are the focal lengths in *u* and *v* directions and (u_c, v_c) is the principal point offset. t_c is the position of the camera centre in an object frame and R_c is the rotation from the camera back to the object frame; p is a *D* point in the object frame. If u_i and v_i denote the measurements of point p_i , the reprojection error ϵ_i is:

$$\epsilon_i = \begin{pmatrix} u_i \\ v_i \end{pmatrix} - \left[\begin{pmatrix} 0 & 0 & 1 \end{pmatrix} KP_c \begin{pmatrix} p_i \\ 1 \end{pmatrix} \right]^{-1} \begin{pmatrix} 1 & 0 & 0 \\ 0 & 1 & 0 \end{pmatrix} KP_c \begin{pmatrix} p_i \\ 1 \end{pmatrix}$$

The images dataset and GNSS measurement that minimizes the residues on GCPs and the reprojection errors will be refined by removing the Tie-Points with greater reprojection error at a chosen threshold.

The frequency distribution of reprojection errors can be described as a distribution skewed to the right; in this study, a Weibull distribution was used because it seemed to suit better than others to the distribution of data (Fig. 7).

The Weibull distribution is a continuous probability distribution defined by two main parameters, a shape parameter *a* and a scale parameter *b*. This distribution is related to a number of other probability distributions; in particular, it interpolates between the exponential distribution ($a = 1$) and the Rayleigh distribution ($a = 2$ and $b = \sqrt{2\sigma}$, σ is the standard residue). The estimation of the parameters *a* and *b* of Weibull distribution, the average, the mean of the standard deviation and the residue fitting, were computed with a Matlab Toolbox (Distribution Fitter). To quantify the acceptance threshold value of reprojection error and to eliminate the Tie-Points with error projection above the threshold value, it is possible to calculate the confidence interval of the estimated distribution corresponding to the chosen confidence level.

For this purpose, statistical software can still be used (in Matlab) or, more simply, it is possible to use the Chebyshev's inequality provided value, which allows to fix the amplitude of the confidence interval through a multiple of the standard residue expressed by:

$$\text{Prob} (|X - \mu| \leq \lambda \sigma) \geq 1 - 1 / \lambda^2$$

where, $\lambda \sim 5$ with probability 0.95 e $\lambda = 10$ with probability 0.99. The threshold value chosen to eliminate the outliers is the one corresponding to the 95% confidence level.

5. RESULT AND DISCUSSIONS

5.1 GNSS results

The duration of the session over 5 hours used to connect the Master station to permanent stations guaranteed a high precision in the position of the points, 4 mm in planimetry and 10 mm in altimetry.

From the Master station, the baselines on GCPs were distant at less 50 m and were measured with sessions over 30 min. The computation of the baselines produced RMS in the order of 4 ÷ 5 mm in planimetry and 12 mm in height. The values of the GCPs thus obtained represent the reference values for evaluating the accuracy of the measurements in nRTK mode.

The absolute values of the coordinate differences are on average 15mm in planimetry and 26 mm in altimetry, the associated RMS is 9 mm and 12 mm respectively.

It is noted that the uncertainty provided at the time of the survey in nRTK mode was on average 8 mm in planimetry and 15 mm in altimetry. This result highlights the sufficient reliability of the network measured in nRTK and the assurance of the

precisions provided during the corrections in real time, thus authorizing the use of the nRTK mode for the remaining GCPs.

5.2 Photogrammetric processing

In order to evaluate the different scenarios, the data processing steps were grouped according to the GCPs used for the bundle block adjustment (A - B - C). The following parameters were set for the calculation of point clouds: in the Align Photos phase, Accuracy = High (original photos), Key-Point limit = 4000, Tie-Point limit = 4000. To optimize camera alignment process, f (focal length), c_x and c_y (principal point offset), k_1 , k_2 , k_3 , k_4 (radial distortion coefficients), were fitted.

In the building of the Dense Cloud the parameters used were: Quality = High (1/4 of original photos), Depth filtering = Disable; once the complete elaboration of the photogrammetric shots was done, it created the texturized 3D model of the Avella Amphitheatre, used to extract the nadiral orthophoto, required for the vectorialization of the top view.

Through the various photogrammetric elaborations, all the points measured on the ground were used as GCPs.

Figure 8 shows a perspective view of the dense cloud obtained from the photogrammetric process with the Nadir and Oblique images. For each Tie-Point computed by the software, some accuracy parameters were computed using a Python script, for example, the re-projection error, the projection accuracy and the RMSE on GCP. These parameters were used to evaluate the accuracy of the model, mainly with statistical analysis.

5.3 GCP residuals analysis

The use of Oblique shots was necessary to reduce occlusion in images and to acquire images of vertical elements (i.e. walls) and avoid shadow cones.

In Figure 9 the box plots of the 3D GCP residuals were reported in the two configurations (only Nadir images and Nadir plus Oblique images) for each type of GNSS measurement (Salazar et al., 2015).

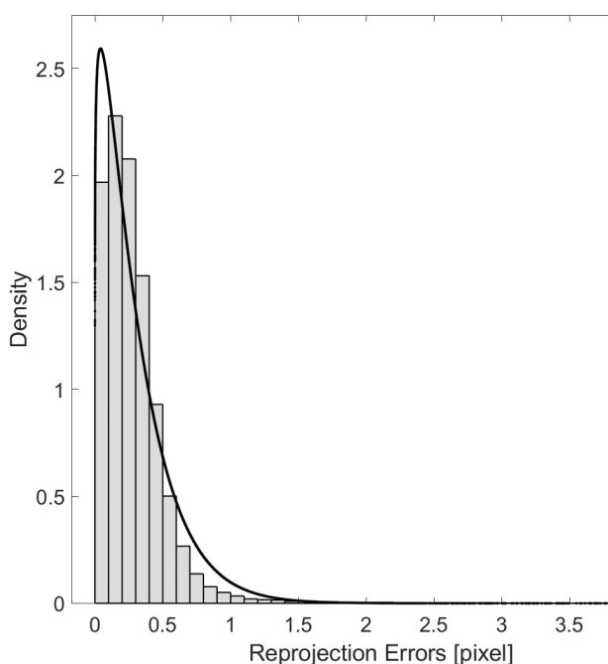


Figure 7: Empirical frequency distribution and its best fit through a Weibull distribution (data: reprojection error of Nadir plus Oblique Static model).



Figure 8: Prospective view of dense cloud.

In this case study, the residuals on the GCPs are more dispersed for the set of Nadir plus Oblique images.

In the processing of the set with only nadiral images, the average residual values with measurements on natural points are slightly higher but less dispersed. Using photogrammetric targets, the interquartile range is smaller, and the lowest residuals are obtained processing the set with only nadiral images.

The test shows that for the set of images with nadiral and Oblique shots, the best result is obtained by fast - static measurements, in other words, with more accurate types of measurements.

However, for the set with only Nadir images, however, the type of measurement got using GNSS techniques has less influence; in fact, the nRTK measurements, both on natural points and on photogrammetric targets, have interquartile range and similar average residues.

Moreover, from the box plots it can be observed that the measurement on photogrammetric targets, or natural points (if well visible on the images) is irrelevant, both in the set with only images Nadir that Nadir plus Oblique. For the Nadir images set, both the maximum error and the minimum error were computed in the nRTK measurement mode on natural points (respectively A6 and A13), while the Nadir plus Oblique image set, the maximum error was computed in the nRTK measurement mode on natural point (A6), the minimum error was computed in the nRTK measurement mode on photogrammetric target (P6). Analysing the following whisker charts, the configurations that respect the graphic error ($0.2\text{mm} \times S = 1\text{cm}$, where S is the representation scale, in our case $S=50$) the acceptable configurations are:

- for the Nadir set the configurations A and C;
- for the Nadir plus Oblique set only configuration A.

For the extraction of the products, necessary for the subsequent vectorization, the chosen configuration is the Nadir plus Oblique images (configuration A), that was the most accurate solution.

5.4 Reprojection error analysis

In Nadir, two the statistical parameters computed on the analysis of reprojection errors are reported: it is possible to observe that the set of nadiral plus Oblique images had minor average reprojection errors in all the corresponding GCP configurations.

By accepting the Weibull distribution for the fitting of reprojection errors, for the Nadir plus Oblique image set, in each GCPs system, frequency distributions have a peak always greater than the homologous one with only.

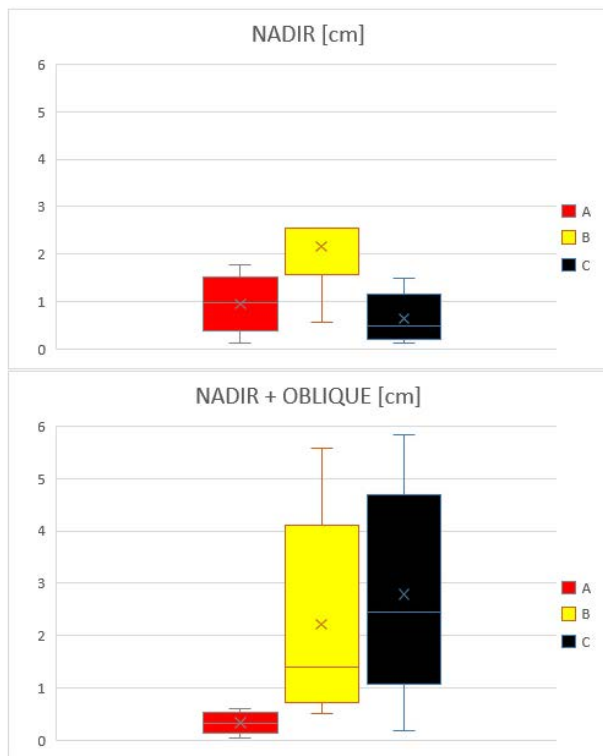


Figure 9: The box plots of the 3D GCP residuals.

Tab. 2: Statistical parameters on the analysis of reprojection errors.

		NADIR [pix]	NADIR plus OBLIQUE [pix]
A	mean	0.59	0.39
	RMSE	0.25	0.13
	95 Percentiles	0.71	0.46
	a [scale par]	0.62	0.4
	b [shape par]	1.17	1.09
	min	0	0
	max	14.4	18.44
B	mean	0.44	0.29
	RMSE	0.14	0.07
	95 Percentiles	0.53	0.35
	a [scale par]	0.47	0.31
	b [shape par]	1.16	1.12
	min	0	0
	max	14.35	18.43
C	mean	0.46	0.31
	RMSE	0.15	0.08
	95 Percentiles	0.55	0.37
	a [scale par]	0.49	0.33
	b [shape par]	1.18	1.13
	min	0	0
	max	14.29	18.36

Nadir images (Fig. 10), that is, for configurations with Oblique images, the number of Tie-Points with low reprojection error is greater. It is possible to estimate the metric reliability of the error projection by multiplying this value by the average GSD. The analysis conducted show that the accuracy of the GNSS measurement on GCPs has a greater influence on the bundle adjustment process, compared to the number of measured points.

5.5 Cloud to cloud comparison

The comparison between the point clouds computed by only nadiral and nadiral plus Oblique shots, with GCP measured in fast-static mode, was performed.

Figure 11 shows that the major differences between the point clouds are contained within the uncertainty of the GCPs measurement (1 cm). The greatest differences are in correspondence with the metal steps and on the shadow zones the latter present in the dataset of the only Nadir photogrammetric shots.

Figure 12 shows a detail of the southeast area (Fig. 11, square outlined in black). It is observed that only with the integration of Oblique shots it is possible to reconstruct the vertical walls, not computed by the nadiral shots only.

In Figure 12, from the processing with Nadir plus Oblique images, it is possible to note the total 3D reconstruction of the mosaic on the vertical walls (both floors of the arena and the *ima cavea*, and the *ima cavea* and the *media cavea*).

The vertical walls are not reconstructed in the 3D model with only Nadir images, due to lack of data.

The modality that minimizes both residues (on GCPs and reprojection errors) is obtained from Nadir plus Oblique frames, with GCP measured in static mode.

An orthoimage is obtained from the processing in order to realize a vector top view at 1:50 scale.

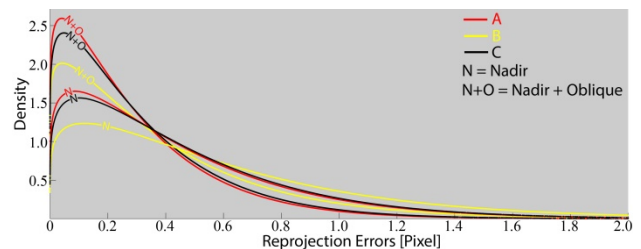


Figure 10: Weibull distributions of reprojection errors.

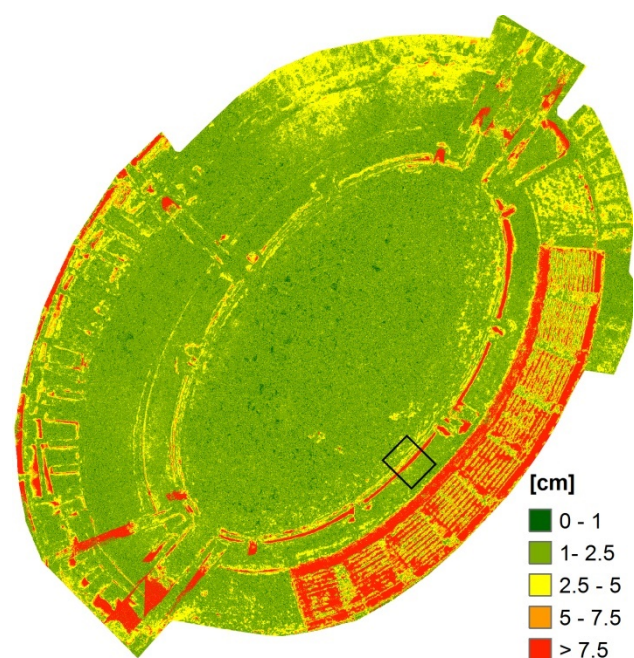
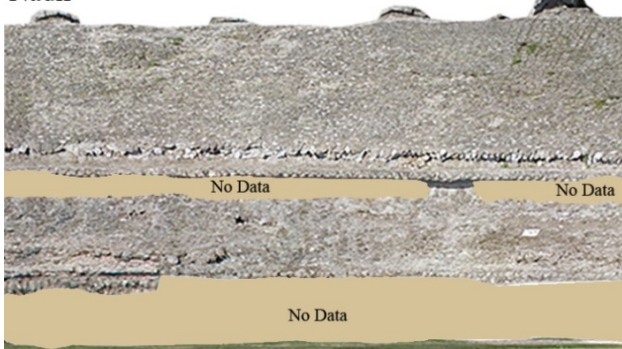


Figure 11: Nadir plus Oblique vs Nadir.

Nadir



Nadir + Oblique



Figure 12: Detail of a section.

6. CONCLUSIONS

Observing the residues on the GCPs, the photogrammetric set appears more stable employing only nadir frames. In the case study, the GCP measurement shows that the nRTK technique allows results comparable to those obtained with static measurements, both in precision and reliability (< 2.5 cm).

The two images acquisition modes, georeferenced on the same GCPs are compared.

The results reveal that most of the discrepancies between the point clouds are contained within the uncertainty of the GCPs measurement (1cm). The accuracy of the models is also evaluated through the reprojection errors. The empirical trend of the error follows a Weibull frequencies distribution. The estimation of the parameters that characterize the best-fit distribution for the experimental data (in different combinations of acquisition and GCP measurement) guarantee two results. The first one is the identification of a confidence range for the distribution in order to eliminate points with an error that is outside the defined gap. The second one is the recognition of the solution with the greatest frequency of small reprojection errors.

Reprojection errors is always smaller in the Nadir and Oblique image set than the homologue with Nadir-only image sets.

Finally, it is observed that, with GCPs measured in nRTK mode, respecting the graphical error, the maximum representation scale is 1:100, while only with GCP measurements in static mode it is possible to describe major details, at a scale of 1:50.

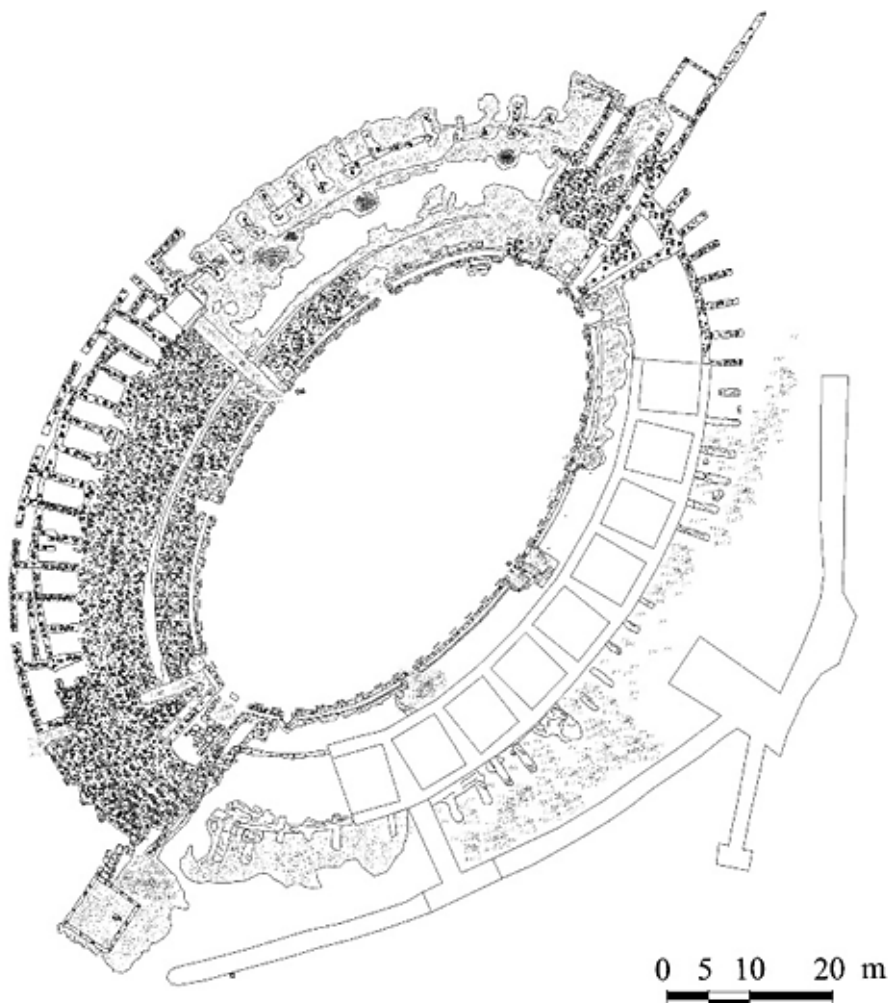


Figure 13: Top view of the Amphitheatre of Avella (edited by Francesco Mele in scale 1:50).

ACKNOWLEDGEMENTS

The Avella's Project was supported by *Soprintendenza Archeologica, Belle Arti e Paesaggio per le province di Salerno e Avellino*. The authors would like to thank the drone pilot Rocco D'Auria (RDigital) for the collaboration in the images acquisition by the UAV.

REFERENCES

- Agarwal, S., Snavely, N., Seitz, S.M. and Szeliski, R., 2010. Bundle Adjustment in the Large. In: Daniilidis, K., Maragos, P. and Paragios, N. (eds.), ECCV 2010, Part II. LNCS, vol. 6312, Springer, 29-42.
- Agisoft LLC, 2017. *Agisoft PhotoScan User Manual*. Version 1.3, Agisoft, 105.
- Banda, H., Chiabrando, F., Giulio Tonolo, F. and Marenchino, D., 2007. Mapping of archeological areas using a low-cost UAV the augusta bagienorum test site. Proceedings of the XXI International CIPA Symposium, Athens.
- Barbarella, M., 2014. *Digital technology and geodetic infrastructures in Italian cartography*, Città e Storia, Volume 9, Issue 1, 91-110.
- Bilis, T., Kouimtoglou, T., Magnisali, M. and Tokmakidis, P., 2017. The Use of 3D Scanning and Photogrammetry Techniques in the Case Study of the Roman Theatre of Nikopolis. Surveying, Virtual Reconstruction and Restoration Study. In: *The International Archives of Photogrammetry, Remote Sensing and Spatial Information Sciences*, 42, 97.
- Borlin, N., Lindstrom, P. and Eriksson, J., 2003. A globally convergent Gauss-Newton algorithm for the bundle adjustment problem with functional constraints. In: Gruen, A. and Kahmen, H. (eds), Optical 3-D Measurement Techniques VI, Vol. 2, Wichmann-Verlag, 269-276.
- Cardone, V., 2015. *Modelli grafici dell'architettura e del territorio*, Maggioli Editore, 288-297.
- Eisenbeiß, H., 2009. *UAV Photogrammetry*, doctorate, ETH Zurich, 237.
- Fiorillo, F., De Feo, E. and Musmeci, D., 2016. The architecture, geometry and representation of the Amphitheatre of Pompeii. In: *The reasons of Drawing*, Gangemi Editore, 1143-1146.
- Irschara A., Kaufmann V., Klopschitz M., Bischof H, and Leberl F., 2010. Towards fully automatic photogrammetric reconstruction using digital images taken from UAVs. *ISPRS - Advancing Remote Sensing Science*.
- James, M.R., Robson, S., d'Oleire-Oltmanns, S. and Niethammer U., 2017. Optimising UAV topographic surveys processed with structure-from-motion: Ground control quality, quantity and bundle adjustment. In: *Geomorphology*, 280, 51-66.
- Kume, H., Taketomi, T., Sato, T. and Yokoya, N., 2010. Extrinsic camera parameter estimation using video images and GPS considering GPS positioning accuracy. In: *International Conference on Pattern Recognition*, 3923-3926.
- Limongiello, M., Santoriello, A., Schirru, G., Bonaudo, R. and Barba S., 2017. The Amphitheatre of Avella: from its origin to digital. II International Conference Metrology for Archaeology.
- Lowe, D., 2004. Distinctive image features from scale-invariant keypoints, cascade filtering approach. In: *IJCV*, 60, 91-110.
- Nocerino, E., Menna, F., Remondino, F. and Saleri, R., 2013. Accuracy and Block Deformation Analysis in Automatic UAV and Terrestrial Photogrammetry - Lessons learnt. In: *ISPRS, Annals of the Photogrammetry, Remote Sensing and Spatial Information Sciences*, II-5/W1, 203-208.
- Remondino, F., Barazzetti, L., Nex, F., Scaioni, M. and Sarazi, D., 2011. UAV photogrammetry for mapping and 3D modelling-current status and future perspectives. In: *Proceedings of the ISPRS - The International Archives of the Photogrammetry, Remote Sensing and Spatial Information Sciences*, vol. XXXVIII-1/C22, ISPRS Workshop, Zurich, 14-16 September, Zurich, Switzerland, 25-31.
- Rinaudo, F., Chiabrando, F., Lingua, A. and Spanò, A., 2012. Archaeological site monitoring: UAV photogrammetry can be an answer. In: *International Archives of the Photogrammetry, Remote Sensing, and Spatial Information Sciences*, vol. 39, N. B5, 583-588.
- Rothermel, M., Wenzel, K., Fritsch, D. and Haala, N., 2012. SURE: Photogrammetric Surface, Reconstruction from Imagery. *Proceedings LC3D Workshop*.
- Salazar, S., Eliana, B., Suspichiatti, R., Rossi, G.S. and Barba, S., 2015. Fotogrametría digital terrestre versus escáner láser: metodología y análisis métrico. *Agrimensura 2015*, La Habana, 15.
- Saleri, R., Cappellini, V., Nony, N., De Luca, L., Marc Pierrot-Deseilligny, M. P., Bardiere, E. and Campi, M., 2013. UAV photogrammetry for archaeological survey: The theaters area of Pompeii. In: *Proceeding of International Congress of DigitalHeritage*, vol. 2. Marseille, 497-502.
- Schneider, C.T., 1991. 3-D Vermessung von Oberflächen und Bauteilen durch Photogrammetrie und Bildverarbeitung. In: *Proceedings IDENT/VISION '91*, Stuttgart, 90-93.
- Verhoeven, G. and Docter R., 2013. The amphitheatre of Carnuntum: towards a complete 3D model using airborne Structure from Motion and dense image matching. In: *10th International Conference on Archaeological Prospection*, 438-440.